Fermi National Accelerator Laboratory

FN-405
2125.000

HADRON CALORIMETRY AT THE FERMILAB TAGGED PHOTON SPECTROMETER FACILITY

J. A. Appel, P. M. Mantsch, and M. M. Streetman
Fermi National Accelerator Laboratory
Batavia, Illinois 60510

and

R. M. Robertson
University of Oklahoma
Norman, Oklahoma 73069

July 1984

Operated by Universities Research Association Inc. under contract with the United States Department of Energy

Hadron Calorimetry at the Fermilab Tagged Photon Spectrometer Facility

J. A. Appel, P. M. Mantsch, and M. M. Streetman
Fermi National Accelerator Laboratory*
Batavia, Illinois 60510, U.S.A.

R. M. Robertson+
University of Oklahoma*
Norman, Oklahoma 73069, U.S.A.

ABSTRACT

Hadron calorimetry apparatus and techniques as used in the Fermilab Tagged Photon Spectrometer Facility are described. This paper concentrates on the iron-acrylic scintillator device which is used in conjunction with an upstream lead-scintillator electromagnetic shower calorimeter. Distributions of energy deposit are given which can be used for Monte Carlo simulations of hadronic showers in such devices. We also present results on calibration, energy resolution and stability. The uses of the system in triggering on hadronic events in a photon beam and in the observation of neutral hadrons are described.

Introduction

Calorimeters have played an increasingly important role in high energy physics experiments. This is due, first, to the

---

*Work supported by the United States Department of Energy.

+Current Address: Bell Laboratories, Allentown, Pennsylvania.

increased resolution possible with higher energy incident particles and, second, to the increased calorimeter ability to help in selecting rare, but interesting events from the background. Finally, multiparticle spectrometer experiments have increased the need for complete event specification including neutral hadrons.

The use of sampling devices, as energies and the need for larger active areas have increased, is made possible by use of increasingly inexpensive materials. Production techniques and assembly procedures have become more industrial in nature. These characteristics are well illustrated by the two devices used for hadron calorimetry in the Tagged Photon Spectrometer Facility (Figure 1).

The most upstream device is an electromagnetic shower detector called the SLIC (an acronym for Segmented Liquid Ionization Calorimeter). The active cross sectional area of the SLIC is 2.4m high x 4.9m wide. The downstream device, called the Hadrometer, is 2.7m high x 4.9m wide. It was designed to measure that part of the energy from hadronic showers not measured by the SLIC. Less than 1% of the energy of electromagnetic showers reach the Hadrometer.

The SLIC and its use in measuring electromagnetic showers are described in References 1 and 2. In this paper we shall discuss only those features which are relevant to the hadron calorimetry effort.

The Hadrometer is of classic design using hodoscopic scintillators attached to approximately adiabatic light guides which channel the scintillation light to large diameter photomultiplier tubes. The scintillator material is doped acrylic plastic. This material is inexpensive, easily handled and machined, and can be used in self-supporting arrays without the crazing which is characteristic of aromatic scintillator material.

Hadron calorimetry satisfies two needs at the Tagged Photon Spectrometer. First, it is used in preparing a fast trigger for photoproduction of hadronic events. Second, it is used for detection, identification, and energy and angle measurement of neutral hadrons in multiparticle events.

Description of Devices

Hadrons deposit significant energy in the SLIC, the upstream electromagnetic calorimeter. Thus, although designed primarily to measure electromagnetic showers, it is an important element in the analysis of hadrons. The SLIC is a tank of doped mineral oil which contains layers of aluminum clad lead plates. These have teflon-coated channels to direct scintillation light to wavebars located on the perimeter of the active area.

The 20 radiation lengths of metal sheets and scintillator in the SLIC comprise 1.5 absorption lengths of material. This material is divided into 60 equal layers with four sets of readout strips. Horizontal strips are divided into nearly

noncommunicating right and left-hand sides. There are also u and v strips tilted at ±20.5 degrees with respect to the vertical. The light from all 20 layers of a given y, u or v strip is collected in a single wavebar which transmits the light to a photomultiplier tube[3], located at the upstream end of the wavebar. The strips are 3.2 cm wide. Near the center of the SLIC, each wavebar is connected to its own photomultiplier. Beyond 24 y strips and 25 u and v strips, pairs of wavebar share a single photomultiplier. This fine granularity (totaling 334 individual counters) is designed for position definition of high energy photons which shower in the SLIC. The signals from a localized group of these strips are added together to determine the SLIC contribution to a single hadron shower.

The Hadrometer contains 36 layers of 2.5 cm thick steel plate. These plates were especially flattened to within 0.3 cm over their 2.7m high x 4.9m wide area. They are stacked on edge on a 15 cm thick steel slab. The steel and scintillator material together total 6 absorption lengths.

Orthogonal strips of x and y (vertical and horizontal) counters were placed in the 36 gaps in the steel. The scintillator is polymethyl methacrylate doped with 1% naphthalene, 1% PPO, and 0.01% POPOP[4]. This material was selected as the best compromise between the conflicting needs for light output and long attenuation length. The scintillator was cast between sheets of glass which lay in a horizontal position in the production ovens.[5] The glass, 2.5m x 2.5m, was not supported in the middle. The sheets of plastic, nominally 1 cm thick, have

variations of up to ±25%. These variations were systematic, the edges being thinner. Once the sheets were cut into (14.3 cm wide) strips, no detailed selection or matching was performed. However, the first order variations in thickness are calibrated out of the final off-line result by incorporation into a light attenuation correction. On line, both thickness variation and attentuation effects inhibit precision measurements. The strips for the vertical counters had to be augmented in length by solvent bonding a 30 cm piece to one end.

The horizontal and vertical hodoscope elements are located in alternate gaps in the steel. The light from the first nine horizontal strips is collected in undoped acrylic (Type G) light guides as indicated in Figure 1. Similarly, the light from the first nine vertical strips is collected in a light guide for a single photomultiplier tube. This arrangement is repeated for the back 18 gaps.

The classical light guide technique was selected over the less expensive wavebar technique after early tests of sample materials. These tests indicated that a wavebar technique resulted in 1/15 as much signal as a straight run of acrylic scintillator to a photomultiplier tube. Thus, light guides allow for use of a thin acrylic scintillator after each layer of steel. In addition, there is enough light that some effort can be made to reduce the nonuniformities due to light absorption in the scintillator strips. A filter[6] with cutoff at 4150 A, selected for this purpose, was placed between each light guide and photomultiplier tube. The resulting attenuation corrections for

horizontal (y) and vertical (x) counters are indicated in Figure 2. Light from the far end of a counter corresponds to approximately 1.5 photoelectrons for a minimum ionizing particle traversing a single strip. Approximately twice as much signal results from a similar particle traversing the scintillator near the photomultiplier end. The face of the photomultiplier tube is masked so that the same signal results from each of the nine strips. This required reducing light from the center strip by half the unmasked value.

The photomultiplier tube selected for the Hadrometer is a nine-stage cesium antimony dynode, bialkyli photocathode device.[7] These photomultiplier tubes were selected on the basis of their insensitivity to light level and rate effects, acceptable photocathode uniformity, and cost. The photomultiplier tubes are operated with negative high voltage supplies so that the anode signal is dc coupled to the charge integrating ADC readout device.[8] This, in turn, required that the light guide be wrapped with metal foil maintained at the photocathode potential to minimize leakage currents across the face of the photomultiplier tube. The scintillator is similarly wrapped in a reflective aluminum foil which, however, is electrically floated from the photocathode potential. These aluminum foil wrapped assemblies were then further wrapped with 0.1 mm mylar to provide physical and electrical isolation of the aluminum foil from the steel plates of the Hadrometer. Special attention was required to prevent the arcing from the aluminum foil to the steel of the calorimeter. Although the aluminum foil provides optical

isolation from counter to counter, the final light tighting of the counters is provided at the outer surface of the entire detector.

The high voltage divider chain circuit diagram is indicated in Figure 3. This nonlinear chain was selected to maximize linearity. The transistors across the last stages of the chain perform two services. They reduce rate effects to less than 2% at average anode currents up to 50 microamps and reduce nonlinearities by a factor of two. The gain of the nine stage photomultiplier tube is kept low ($4x10^5$) in order to insure linearity of response over a large dynamic range. Peak output currents are 40 microamps per GeV of deposited energy and the outputs have a FWHM of 50 nsec.

The anode signal from each channel of the SLIC and Hadrometer is individually integrated in a charge sensitive ADC.[8] The integration time for the SLIC is 165 nsec and for the Hadrometer, 250 nsec. These ADCs are operated with a least count sensitivity of about 50 MeV.[9] In order to make use of this precision, it is necessary to monitor and correct for pedestal (zero signal level in the ADCs) and to minimize RF noise and electrical ground loop contributions. A single output count in the SLIC and Hadrometer ADCs corresponds to 100 fC and 50 fC, respectively. These values of charge correspond to dc levels of 0.6 microvolts and 0.2 microvolts of dc voltage during the integration time of the devices. Each input coaxial signal cable was wrapped around ferrite cores[10] to reduce the effects of pickup on the cable shield. In order to reduce ground loop

currents to a minimum, the ADC's are operated in a quasi-differential mode, the signal return being isolated from dc ground on each ADC module by 1K ohm.

A signal is also taken from the last dynode of the front y counters. This output is transformer-coupled to prevent ground loops when it is connected to the fast trigger electrical circuitry. Finally, the high voltage returns contain 150 ohms in each line. This results in a small dc voltage with respect to dc ground for each input channel of the ADC system. High voltage is supplied to the divider chains from local dc grounded computer controlled supplies.[11] The pedestal values observed in each channel change by one or more counts in a typical one hour period. The source of these changes has never been isolated. However, by continously monitoring the pedestal values using dummy strobes, it is possible to predict a pedestal value to about 1.5 count rms.

Calibration and Stability

The relative calibration of each of the 142 elements of the Hadrometer is maintained by using special muon calibration data. The muons result from the absorption of the primary proton beam upstream of the experimental area. Once every three weeks during the experiment, the normal photon beam was turned off and triggers were set up for the calibration. No intermediate data are necessary since the calibration values are stable except for an average reduction in sensitivity of about 1/2% per week.[12]

The spectrum of light-attenuation corrected muon signals from the upstream vertical elements is shown in Figure 4. For a muon at the end of the scintillator opposite the photomultiplier tube, the signal typically corresponds to 20 counts from the ADC. The distribution of signals making up this mean value have a FWHM of 60%. For a muon equivalent shower energy of 1.2 GeV, this corresponds to 26 photoelectrons per GeV in a hadronic shower including both x and y detector elements. As will be seen later, even at the far end, the statistical fluctuations in number of photoelectrons (photostatistics) do not contribute significantly to the overall resolution of the device.

Even for events where the position of a hadronic shower in the device is well known and an attenuation correction is applied, there is an additional resolution contribution from the systematic effects of using a not quite correct attenuation curve for each channel. The average shapes of Fig. 2 were used for all counters. By studying the data for individual counter positions, we conclude that the systematic errors introduced by these

standardized shapes are less than 5% in energy resolution.

The absolute overall calibration of the Hadrometer is obtained by minimizing the energy resolution of the combined Hadrometer and SLIC subject to the constraint that the combined signals equal the measured momentum of incident charged hadrons. This technique also provides a measurement of the ratio of SLIC response to hadronic shower energy relative to its response to electromagnetic shower energy. The value of this ratio (.75) is typical of lead scintillator calorimeters. The absolute calibration is insensitive to the angle of incidence of the hadron. Note that the fractional sampling of the device is approximately constant (i.e. independent of angle). Only the sampling frequency and, therefore, resolution changes slightly. Thus, the calibration constants (G_S and G_H for the SLIC and Hadrometer respectively) were determined by minimizing the expression

$$[p - (G_S E_S + G_H E_H)]^2 \qquad (1)$$

where the measured incident hadron momentum is p and the attenuation corrected signals are E_S and E_H.

The muon relative calibration technique suffers from the smallness of the (equivalent 1.2 GeV) signals used. Furthermore, the adjustment for absolute calibration requires that the entire system have a linear response since the overall normalization is made once for the entire device. These two problems were recognized at the beginning and were the motivating factors which led to particular care in selecting photomultiplier tubes, noise

suppression circuitry, and ADC devices. We find the muon based calibration to be significantly more stable than that from a laser based light fiber distribution system which was intended to monitor gains of individual channels. In addition, the muon technique guarantees that the calibration will have as much in common with the physics data as possible. The muon data also provides measurement of the light attenuation along the detector elements.

Charged Particle Performance

Calorimetry is executed by treating the SLIC and two-layered Hadrometer as a single two-layered device. There exist large fluctuations in the fraction of energy deposited in each layer. Typically, just over half the hadrons have more than ionization energy loss in the SLIC. This fraction increases with energy as indicated in Figure 5. Those hadrons which do have showering interactions in the SLIC have large fluctuations in the fraction of energy deposited there. The spectrum of these fractional deposits is evident in Figure 6 for selected ranges of incident hadron momentum.

The hadronic shower energy not deposited in the SLIC appears in the Hadrometer. On average, all but 12% of the primary hadron energy appears in the upstream Hadrometer layer—independent of the incident energy. About half the incident hadrons deposit effectively all their energy in the SLIC and upstream Hadrometer. The half of the hadrons which do deposit shower energy in the

downstream Hadrometer layer leave only the trailing edge of their energy in that last layer. Because the amount of energy in the downstream Hadrometer layer is small and the fluctuation is large, it is combined with the upstream Hadrometer layer in the reconstruction analysis used for calorimetry.

Figure 7 shows the transverse distribution of hadronic shower energy in the layers. In each SLIC (Hadrometer) layer the transverse energy distribution is normalized to the total energy deposited in thirteen (three) counters so that the area under each curve is slightly greater than unity. Also, the distributions give the fraction of energy deposited in a given counter when the trajectory of the incident hadron is the indicated distance from the center of that counter. The distributions differ, therefore, from the ´shower shape´ due to the granularity of the counters. The trajectory is extrapolated to a plane at the face of each counter layer. As is apparent in the figure, the normalized shapes are approximately independent of the energy of the incident particle, but depend on the angle of incidence of the trajectory.

All these longitudinal and transverse energy distributions are taken from isolated (i.e., physically separated in space) showers. Although the distributions depend slightly on the definition of "isolated," when suitably smeared by the energy resolution in each element, they can be effectively used to generate events for analysis code development and to predict the performance of similar devices.

Shower energy contributions from the SLIC are obtained as part of a recursive analysis described elsewhere.[2] The energy of an isolated shower is taken to be the sum of the energy deposit in each layer. In each layer the energy is taken to be the weighted average of the two or three views.

The fractional distribution of energy deposit in the SLIC and Hadrometer can be seen in Fig. 8 for 30 GeV/c incident hadrons and muons. In the regions labelled SLIC dominated and Hadrometer dominated, there is a tendency for the energy measurement to be higher than the momemtum. This is due, in part, to the fact that the energy measurement in neither device is allowed to go negative. The showers in these regions cause the assymetric high tail in the E/p distribution shown in Fig. 9a. The high tail can be artificially removed by substracting from the measured signal an amount corresponding to 13%. This helps reduce the high tails as seen in Fig. 9b. This correction does not significantly affect the full width at half maximum which is used to describe the achieved energy resolution in what follows.

The achieved energy resolution is as indicated in Figures 10 and 11. The resolution is found to be independent of the fractional energy deposition in each layer. It is described well by the expression[13]

$$\frac{\sigma_E}{E} = \frac{75\%}{\sqrt{E}} \qquad (2)$$

where σ_E is the FWHM of the E/p distribution divided by 2.36.

The achieved energy resolution averaged over the calorimeter is comparable to that achieved by others in test beams, even when scaled (by $\sqrt{t}$) for the thin sampling thickness (t=2.5cm) for most of this device. Furthermore, photostatistics contributions as indicated by the muon signals contribute only $25\%/\sqrt{E}$ to the above result. The resolution is dominated by fluctuations in sampling and not by such potential hazards as the systematic errors of attenuation correction, photostatistics or other unknown effects. Failure to include the energy in the back half of the Hadrometer (i.e., using only 4.5 absorption lengths) degrades the resolution by 20% (to $90\%/\sqrt{E}$).

In addition to the total energy, the position in the calorimeter of an incident particle can be determined from the energy deposition. The position is calculated from the first moment of the energy distribution, e.g., according to the following expression:

$$x \text{ centroid} = \sum_i x_i E_i / \sum_i E_i \qquad (3)$$

This expression is used for one or more layers where the values x_i are taken as the center of the relevant calorimeter element, and the energy E_i is the energy deposited in that element. As can be seen from Figs. 12 and 13, the position resolution improves with energy but does not get to be better than approximately 4.5 cm, rms. This rms value is obtained using all the events. If one uses a single gaussian as in Figure 13, a smaller value of position uncertainty is obtained, but the single

gaussian is a poor representation of the data. The sum of two gaussians provides a much better fit, but not a very simple description of the resolution. The resolution obtained using the entire calorimeter is better than that from any individual layer alone, even the SLIC layer with its finer (i.e. narrower) elements.

The width of isolated showers can similarly be calculated from the second moment of the energy distribution. It is calculated from the expression, for example,

$$W_y^2 = \sum_i E_i \, (y_{track} - y_i)^2 / \sum_i E_i \qquad (4)$$

The square roots of the average of W_x^2 and W_y^2 in individual and summed layers are given and in Fig. 14 as a function of incident particle momentum. These data are for particles which are isolated in the calorimeter and at nearly normal incidence. Typical squared width distributions used to generate the above curves are shown in Fig. 15.

During the course of the experiment, the SLIC-Hadrometer combination was not used to determine the energies or positions of individual charged hadrons. However, the results reported in this section are expected to apply equally well to neutral hadrons detected in the calorimeter. Criteria for identifying showers, efficiency of cuts, and confidence in results are obtained by direct comparison of the same distributions for neutral hadrons as those discussed in this section for charged hadrons. Where relevant, calorimetric shower centroids are used

in place of projected track locations so that comparisons are appropriate.

Neutral Hadron Detection and Measurement

The method of neutral hadron detection starts with the off-line subtraction from the Hadrometer data of predicted signals for each of the track-reconstructed charged particles. The subtraction corresponds to the incident charged particle energy minus that part detected in the SLIC. Residual signals in the Hadrometer are then identified with neutral hadrons. This identification is made only if the residues are significantly larger than the uncertainties of the subtractions associated with charged particles and if the resultant signals are consistent with hadronic shower distributions in both x and y views. The calculations of the neutral particle energy, position and shower width are made as described for charged hadrons using both the Hadrometer residues and SLIC showers previously found.

As a test of the quality of the results, the width distributions for neutral hadrons may be compared to those of isolated charged hadrons, both from typical multiparticle data (Figure 16). A more compelling demonstration of the capability of the neutral hadron measurement is the observation of phi mesons. These are observed to decay into a pair of neutral hadrons, K_S and K_L. The K_S is detected by its subsequent decay into charged pions. For events with a K_S and an apparent neutral hadron, the effective mass of the K_S and neutral hadron is calculated (using energy and position data from calorimetry for the K_L) and shown in Figure 17. The peak at 1020 MeV corresponds to detected phi mesons. The measured width (36 MeV FWHM, dominated by the K_L energy measurement) agrees with the expected

resolution.

Triggering on Hadronic Events in a Photon Beam

When a high energy photon beam strikes a fixed nuclear target, two classes of interactions occur. The most likely interaction is the production of an electron and positron pair which travel in the direction of the incident photon. The second class of events, in which hadrons are produced, occurs at the rate of less than 0.1% of the sensible rate of the first class. The hadrons are typically produced at a wide range of angles with respect to the incident photon beam. This differing angular distribution and the fact that electrons and positrons will produce electromagnetic showers early in material with high atomic number can be used to separate the two classes of interaction.

All the counter elements of the Hadrometer and those elements of the SLIC which are outside of the horizontal plane are sensitive to hadronic interactions. The magnetic field of the analyzing magnets in the forward spectrometer bends the electron and positron out of the forward direction in a horizontal plane at beam height. In order to avoid inclusion of the energy from such electrons and positrons, the central horizontal SLIC counters are excluded from the sum which is used to identify hadronic interactions.

In principle, the lowest possible threshold for energy coming from the produced hadrons is desired in a trigger in order to be efficient for the highest possible fraction of hadronic interactions. However, electronic noise from the several levels of fan-in circuitry and pickup from the many cables used in the signal transport puts a lower limit on this threshold. There is also some leakage due to electron-positron pairs which end up depositing energy outside the excluded regions. Figure 18 indicates the relative rate of triggers (i.e., the trigger efficiency) as a function of the effective on-line threshold for combined energy in the SLIC and Hadrometer. The actual threshold is 15 to 30 GeV, varying with incident photon energy, but corresponding to 22% of the photon energy. This provided very nearly 100% efficiency for hadronic interactions.

Particle Identification

The lowest mass particles (photons, electrons and positrons) deposit less than 1% of their energy in the Hadrometer. A test on this can be used to identify both electrons and positrons (whose energy is known by their having been tracked through the magnetic field upstream) and the photons which arrive unheralded at the calorimeters. While the electrons and positrons can be identified by the equality of their SLIC energy and their measured momentum, no such test can be performed for the photons. Photons are identified by energy deposit in the SLIC without a charged particle track entering at that location and without

energy deposit in the Hadrometer behind the SLIC deposit. Thus, the Hadrometer is crucial for the positive identification of the photons.

Muons provide very characteristic signals in the SLIC and Hadrometer. These are the signals described in the calibration section. The absolute energy deposit in each layer can be used to identify muons. Figure 6 shows a very clean separation of hadrons from muons (the "showers" near the origin of the scatter plot). Of course, at a few GeV, the separation becomes much less distinct.

Pions, kaons and protons interact slightly differently in the calorimeters, especially near the beginning of the shower. However, the fluctuations in individual shower development are so large that is not possible to use these differences to do particle identification particle by particle.

Conclusion

The Fermilab Tagged Photon Spectrometer Hadrometer makes use of 2.5 cm iron plates and acrylic scintillator (totaling 6 absorption lengths). In combination with the upstream 20 radiation length (1.5 absorption length) electromagnetic shower detector, an energy resolution of $75\%\sqrt{E}$ is achieved for incident hadrons. The energy resolution is dominated by the shower fluctuations and not photo-statistics or calibration and material nonuniformities. Position resolution of a few cm, varying with energy, is also achieved.

The use of these calorimeters in triggering on hadronic events, detecting and measuring neutral hadrons and particle identification in an actual experiment at the Tagged Photon Spectrometer have been described. Details of the detector's use have depended on its energy resolution and segmentation.

Acknowledgements

We are especially indebted to our colleagues of E516 at Fermilab. Without their efforts, none of the results reported in this paper would have been possible. We mention explicity R. Morrison, D. Summers, R. Kennett, B. Denby and V. Bharadwaj who had principle responsibility for the SLIC. Thanks are also due especially to C. Kerns and R. Krull of the Fermilab Physics Department and E. Fay, R. Lenz, N. Lesnieski, R. Davis, S. Smith and others of the Fermilab staff who helped in the procurement, production and installation of the Hadrometer. Special thanks are also due to A. Timm of Nevis Laboratories of Columbia University and to L. Deringer and L. Sedlacek for preparation of this document.

References

1. V. K. Bharadwaj et al. (under preparation) and V. K. Bharadwaj, et al., NIM 155 (1978) 411.

2. D. Summers (under preparation) and D. Summers dissertation, University of California, Santa Barbara, 1984 (unpublished).

3. Types 4902 and 4900 for inner (single strip) and outer (dual strip) counters, respectively, by RCA, Lancaster, Pennsylvania 17604.

4. W. Kienzle, et al., "Scintillator Developments at CERN," NP Internal Report 75-12, 6 October, 1975, CERN, CH-1211 Geneva 23, Switzerland.

5. Polytech, Inc., Owensville, Missouri 65066.

6. Wratten No. 2E by Kodak, Rochester, New York 14650.

7. Type 9791KB by EMI Electronics Limited, Middlesex, England UB3 1HJ. This photomultiplier tube was selected after testing 14 types (including S11 and bialkalai versions) from five vendors.

8. Model 2285A by LeCroy Research Systems, Inc., Spring Valley, New York 10977.

9. This sensitivity corresponds to typical values at the scintillator end far from the photomultiplier.

10. Each cable was attached to 35 turns of RG174 coaxial cable wound around two solid ferrite cores, part number F626-12-05 by PEMAG Central, Elk Grove Village, Illinois 60007. Noise reduction by a factor of approximately 100 was achieved for the worst noise situation.

11. Model HV4032A by LeCroy Research Systems, Inc., Spring Valley, New York 10977.

12. Early in the life of the Hadrometer, the sensitivity fell by about 1% per week. The 1/2% figure corresponds to the effect during the bulk of data taking. After three additional quiescent years, an additional 35% typical loss of sensitivity and somewhat deteriorated attentuation length were observed.

13. The apparent energy resolution improves by up to 20% (i.e., to $60\%/\sqrt{E}$) when one demands that the shower centroid agree well with the extrapolated charged track position.

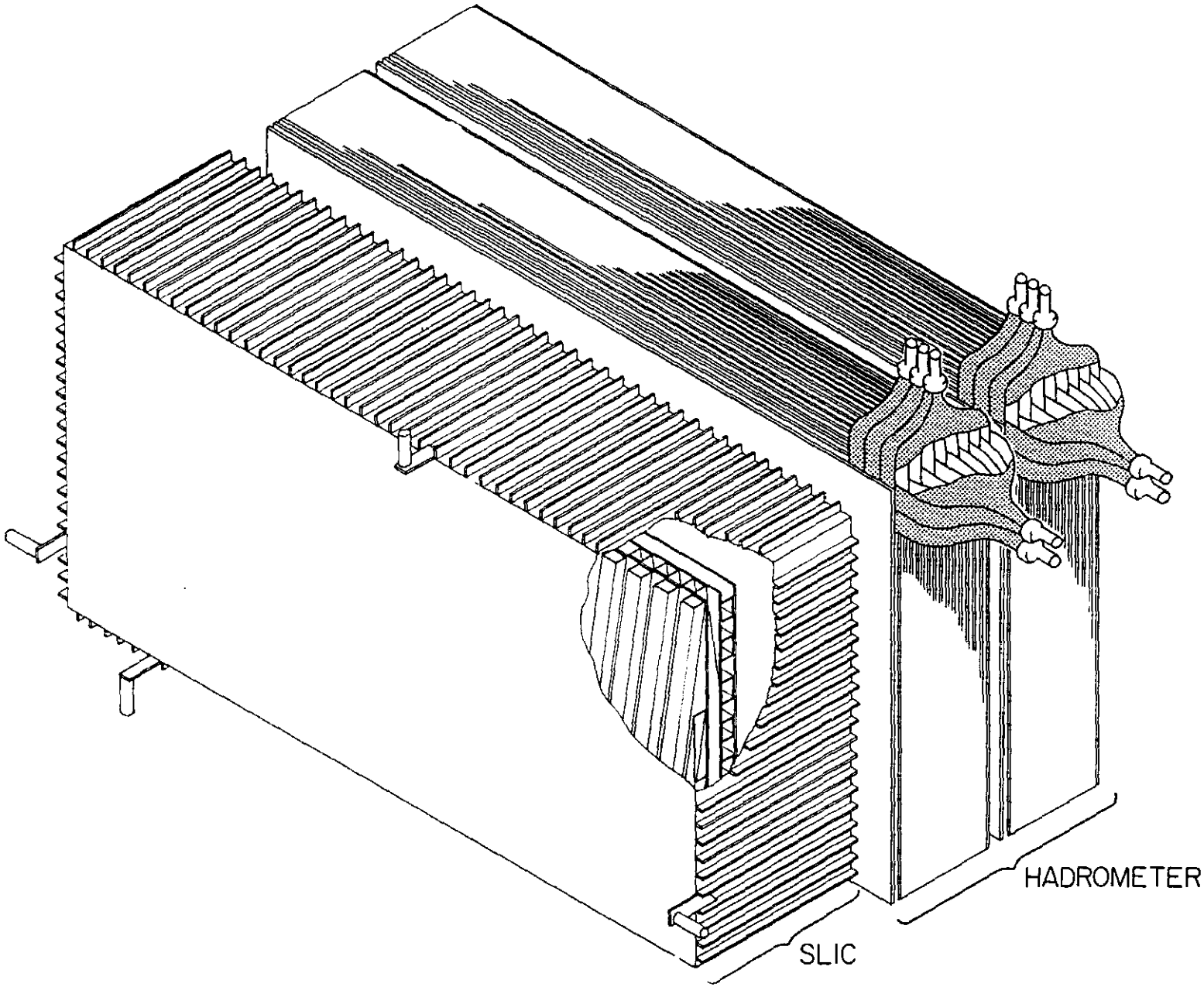

Figure 1

Schematic view of devices used in hadron calorimetry at the Fermilab Tagged Photon Spectrometer facility.

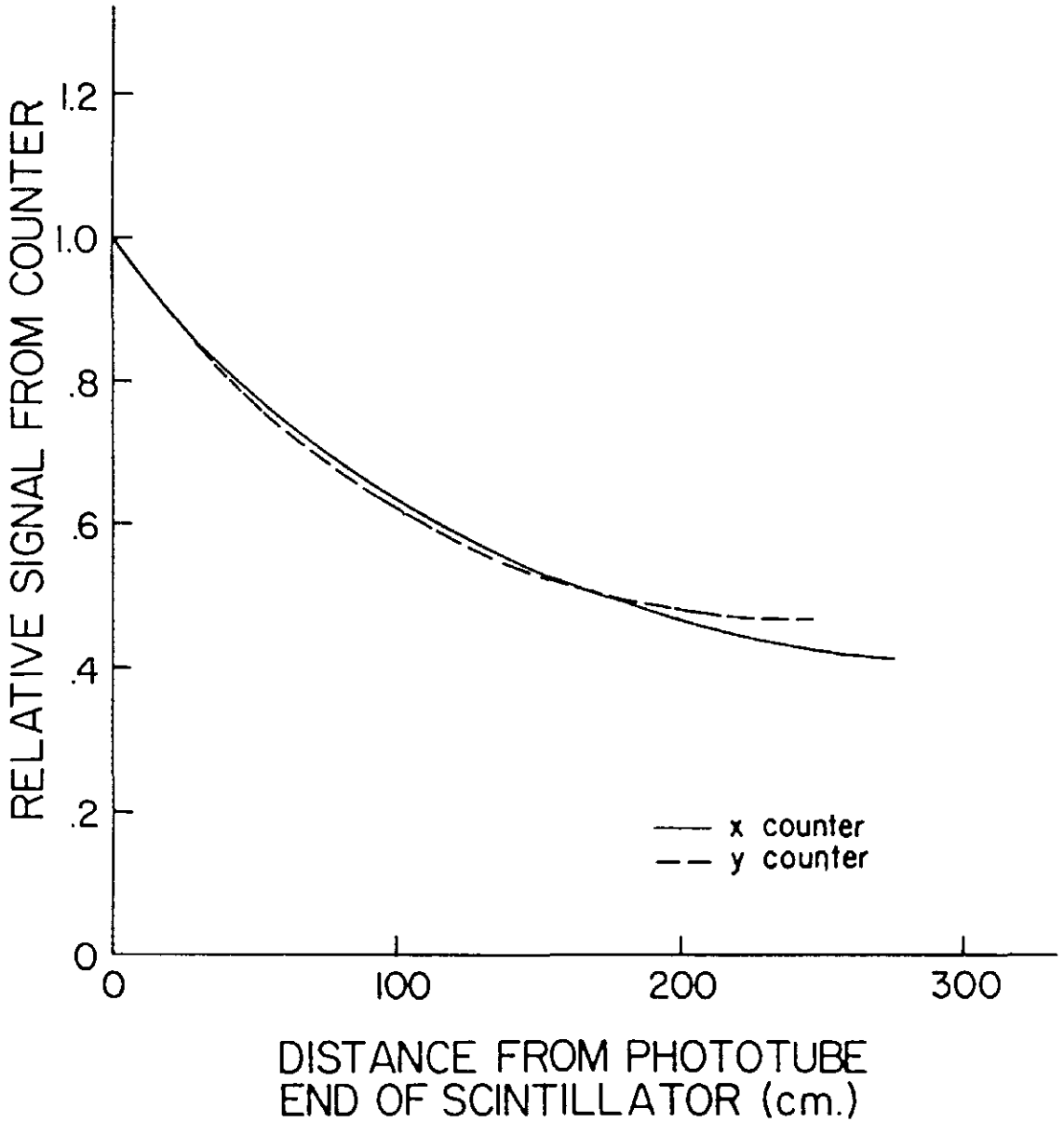

Figure 2

Light attenuation correction curves for Hadrometer counter elements.

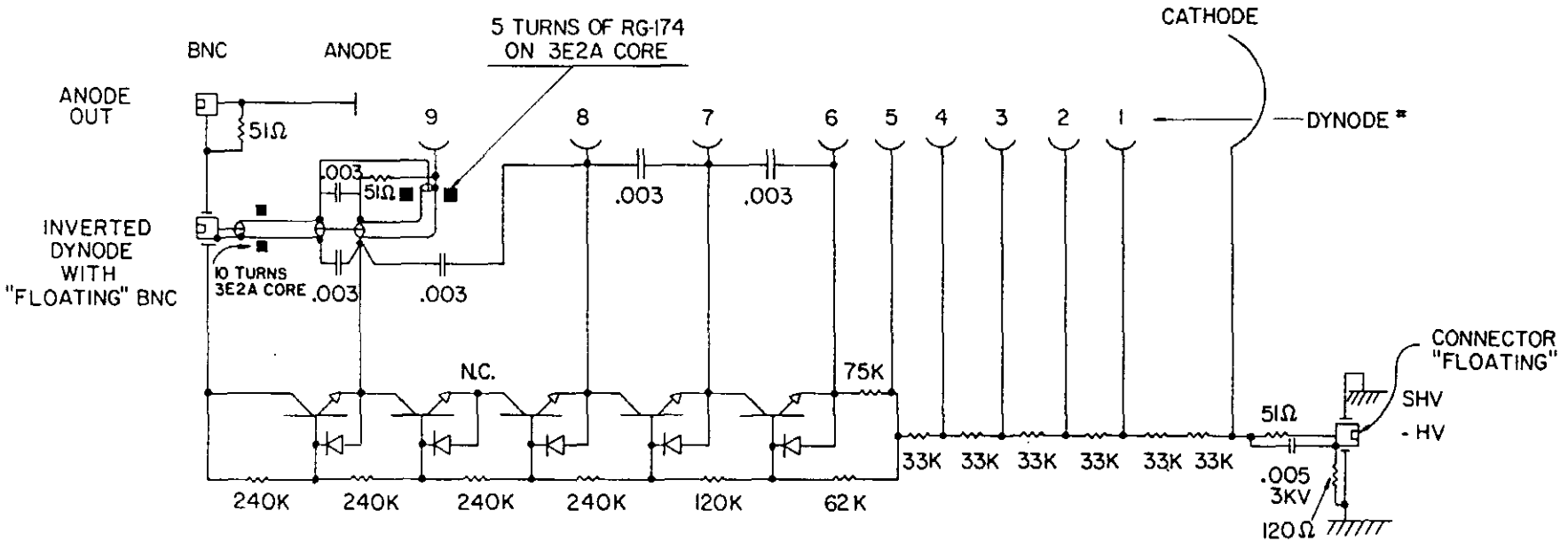

Figure 3

Circuit diagram for high voltage chain and signal outputs used for Hadrometer photomultiplier tubes.

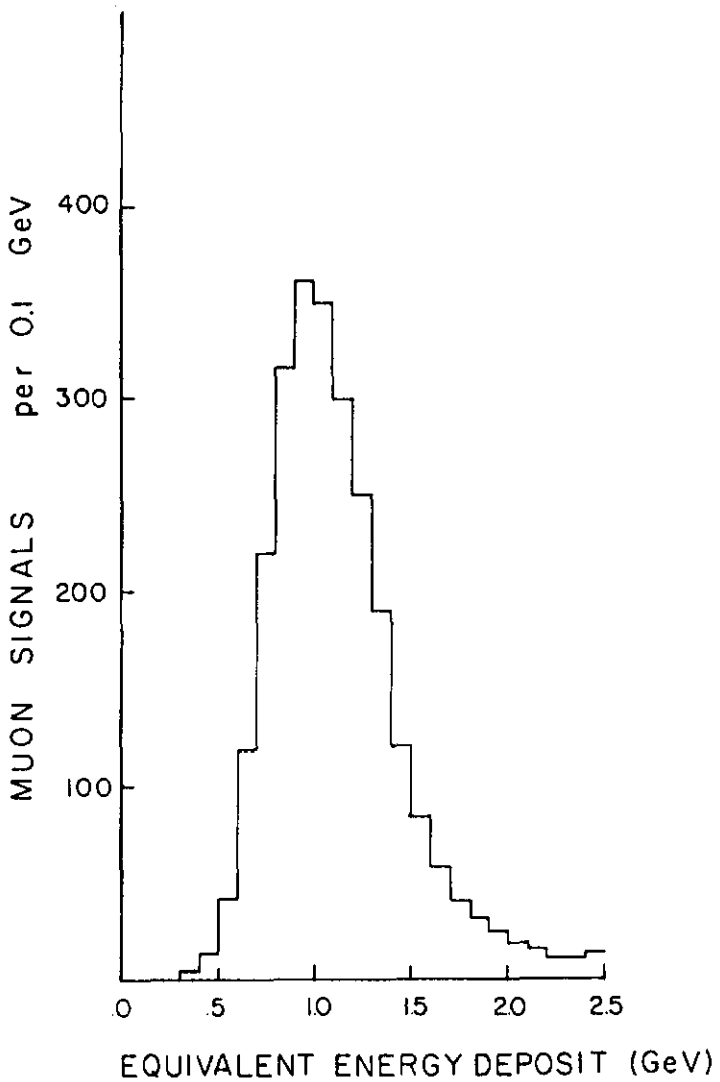

Figure 4

Spectrum of light-attenuation corrected muon signals from the upstream vertical Hadrometer counters.

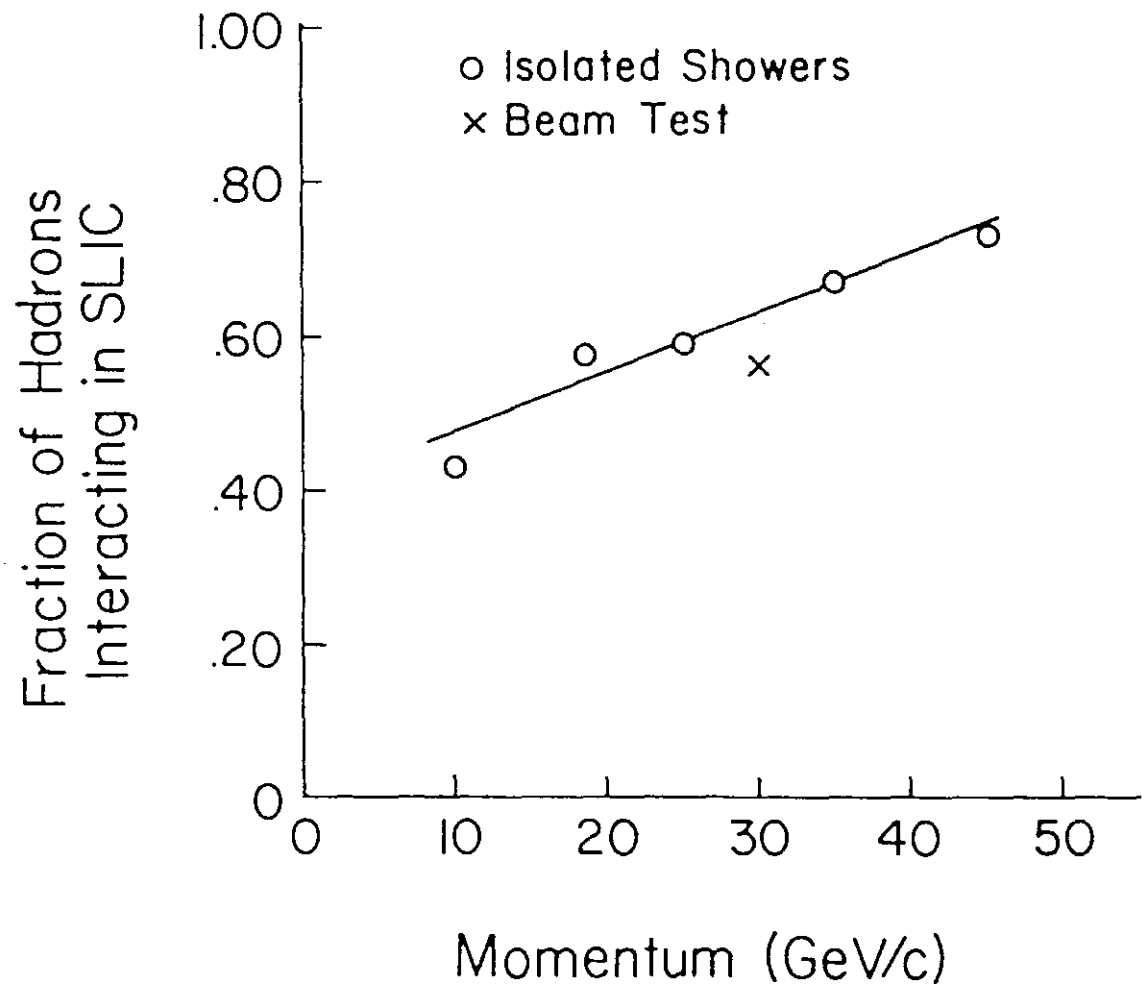

Figure 5

Fraction of 'interacted' hadrons seen in SLIC. Open circles are determined from isolated showers. The X comes from the 30 GeV/c beam test. Normal ionization loss is not considered interacting in this context. See Figure 6.

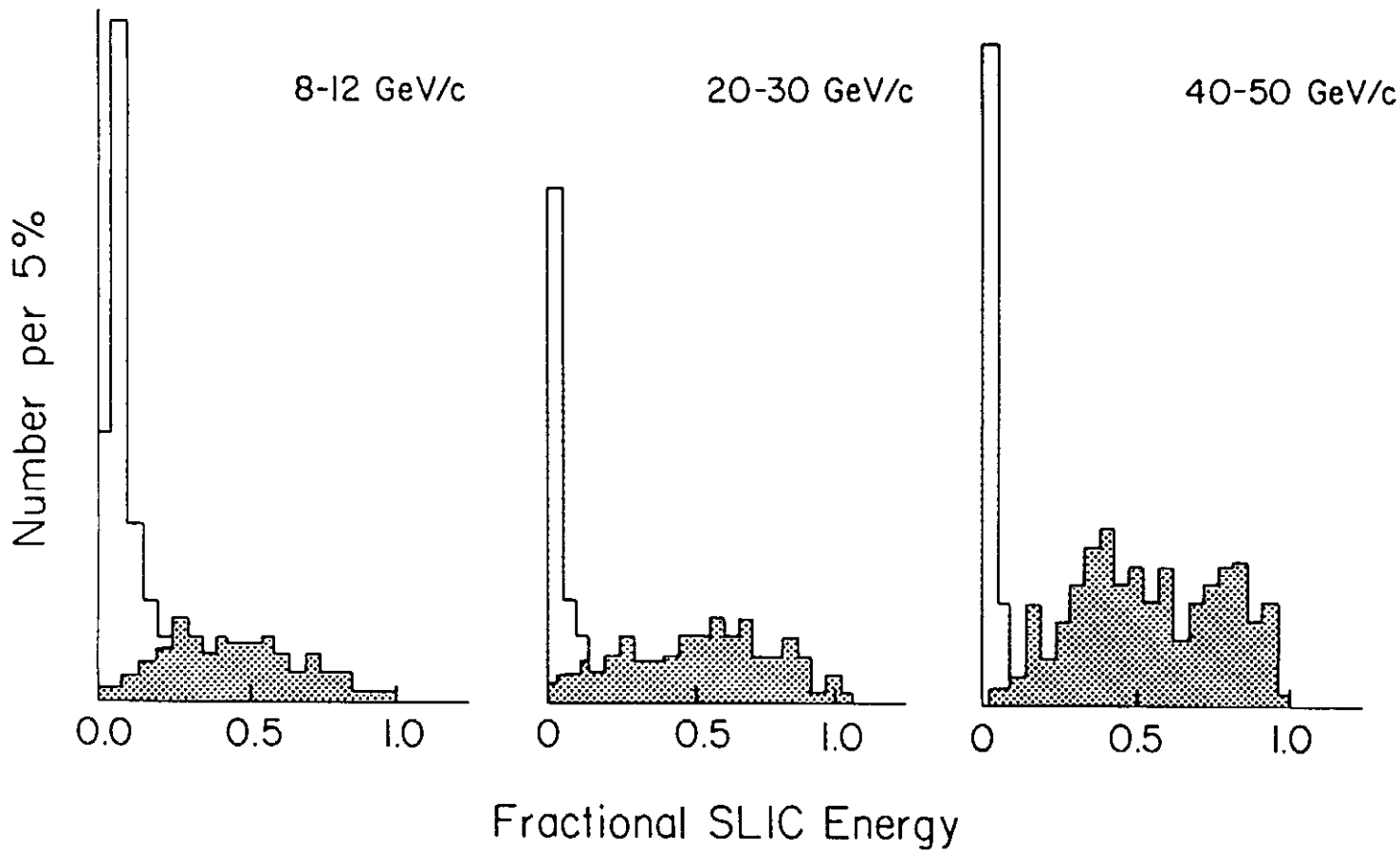

Figure 6

Typical distributions of fractional energy deposit in SLIC for various incident momentum hadrons. The shaded region represents those hadrons considered 'interacted' in Figure 5.

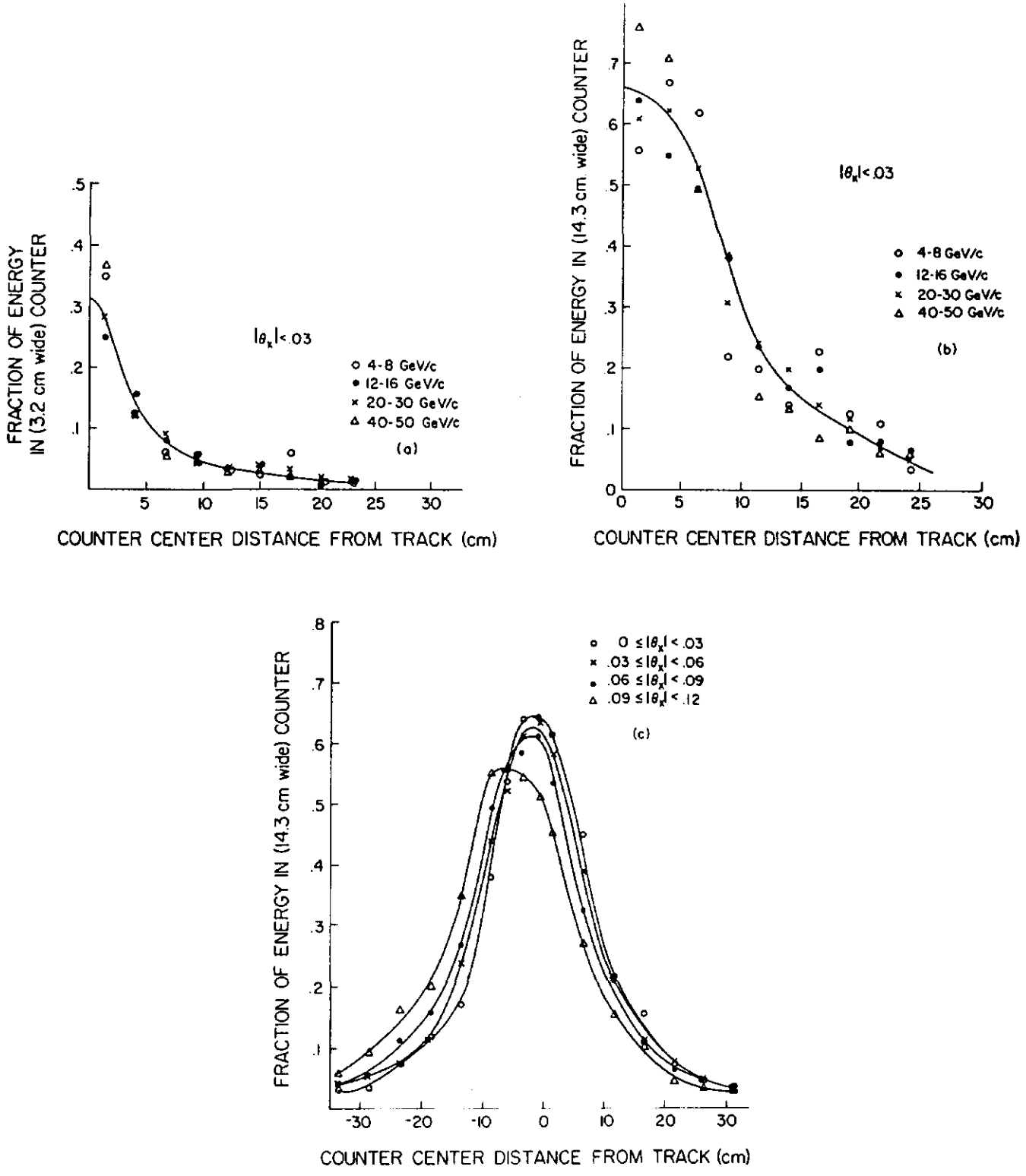

Figure 7

Transverse hadronic shower 'shapes' as seen by elements of the indicated granularity (a) in the SLIC for particles with incident angles (θ) less than .03 from normal and in the Hadrometer vs (b) energy and (c) incident angle.

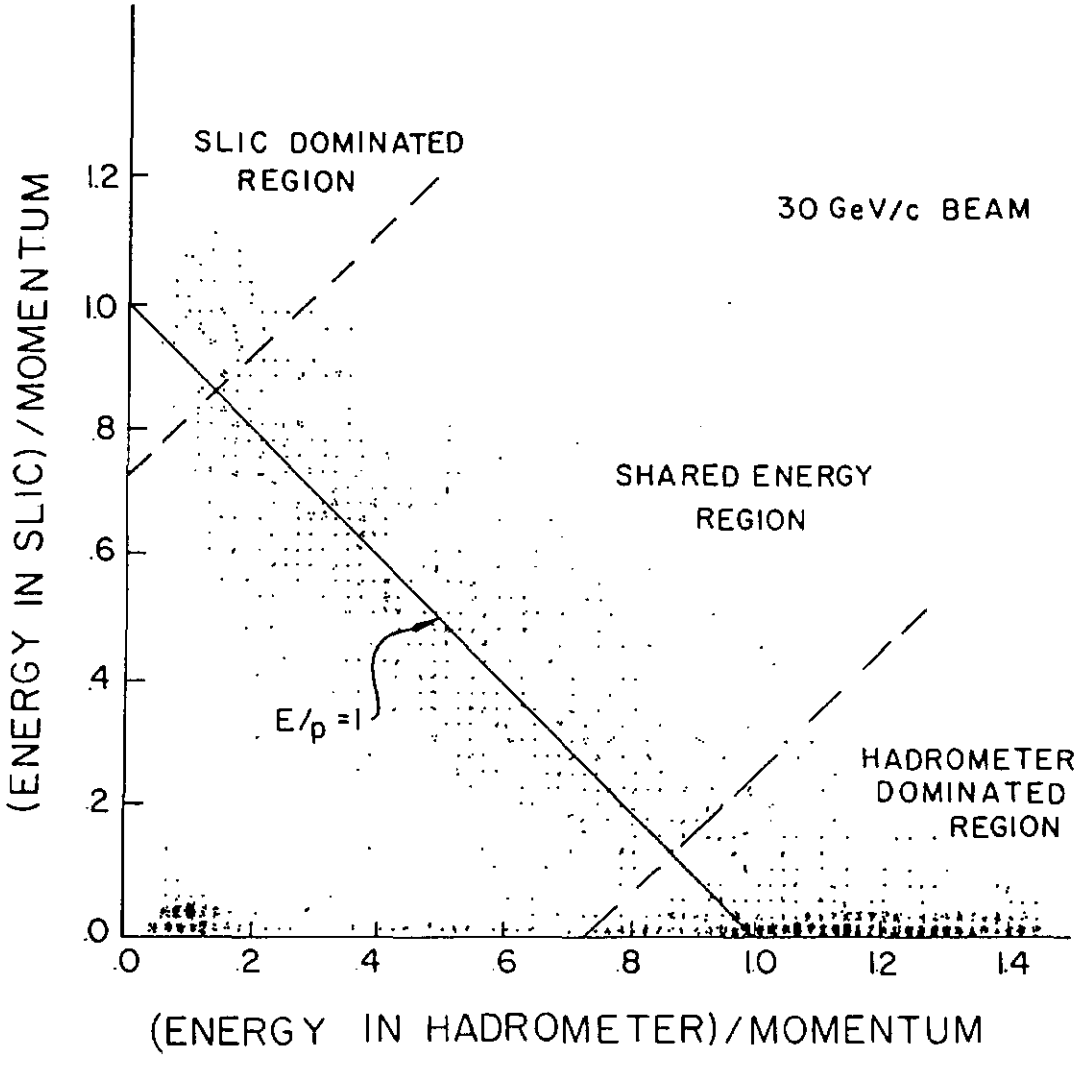

Figure 8

Energy sharing between the SLIC and Hadrometer for 30 GeV hadrons and muons.

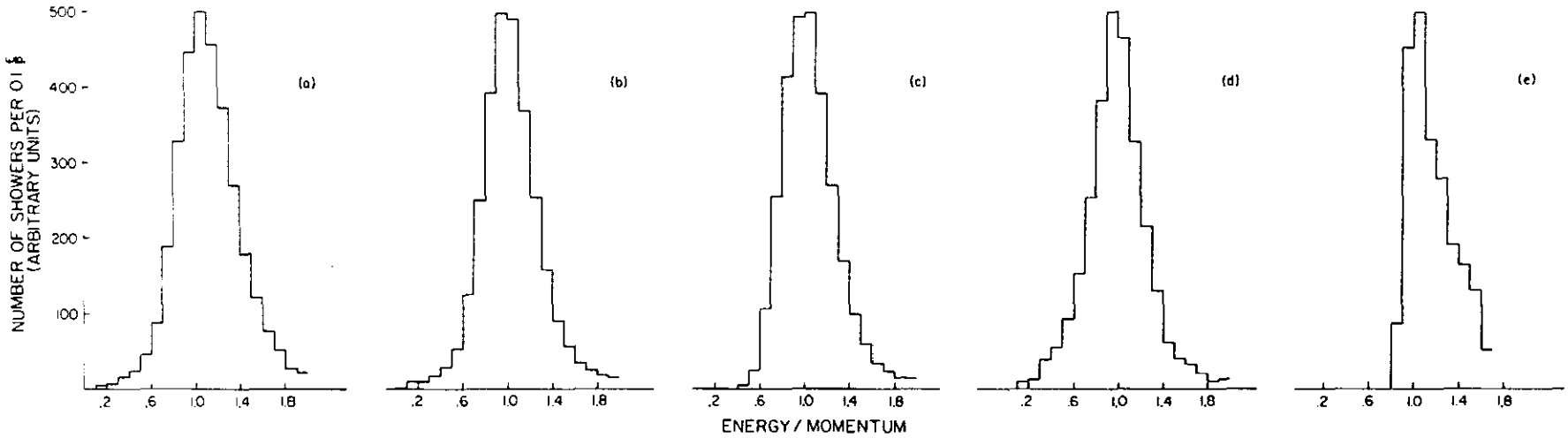

Figure 9

Energy resolution curves (E/p) (a) before tail corrections, (b) following corrections, (c) in Hadrometer dominated region after correction, (d) in shared region and (e) in SLIC dominated region after correction.

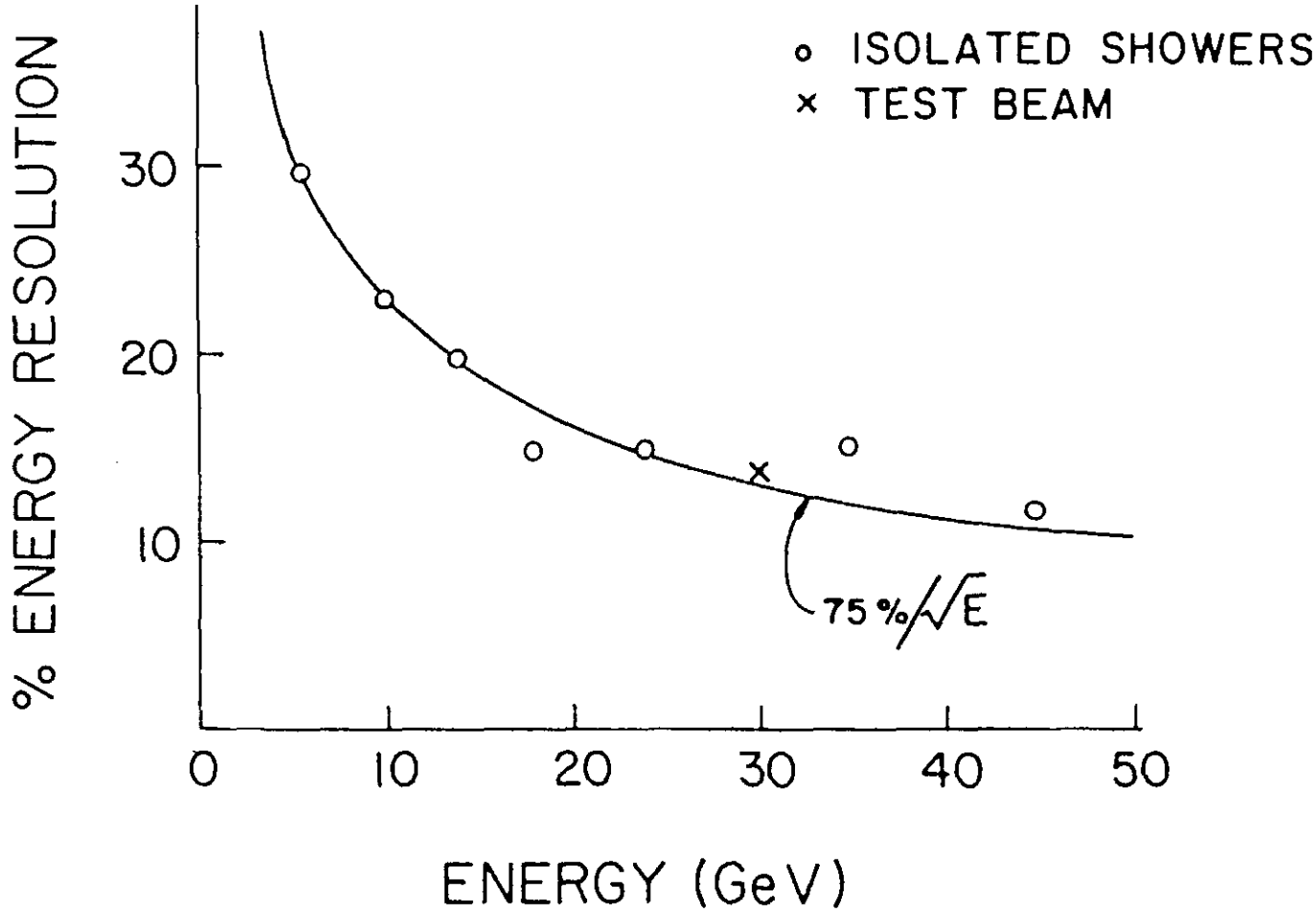

Figure 10

Achieved energy resolution versus energy for isolated showers in multiparticle events. The resolution is presented as the FWHM/2.36 from the E/p distributions like those in Figure 11.

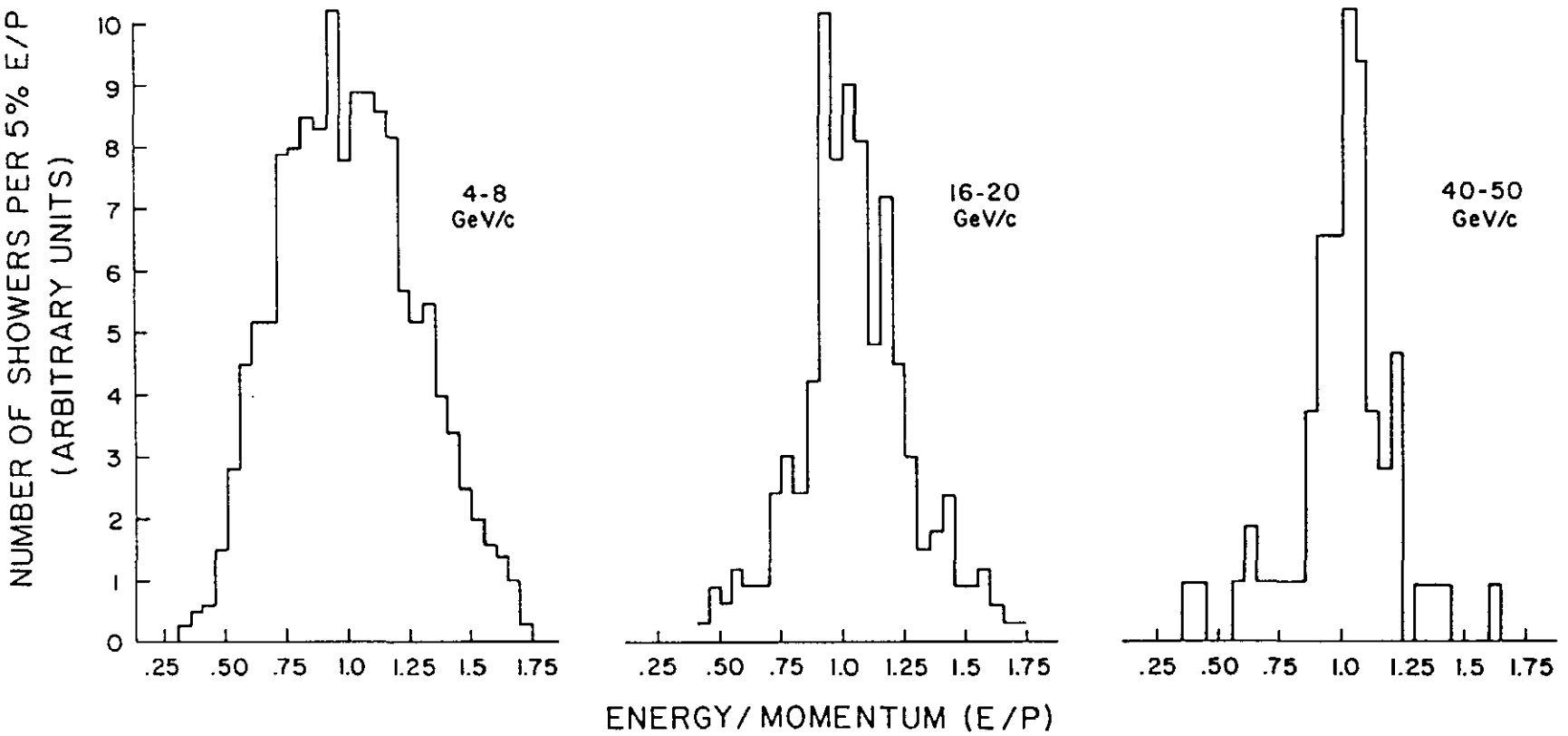

Figure 11

Energy resolution curves (E/p) for hadrons in various momentum ranges.

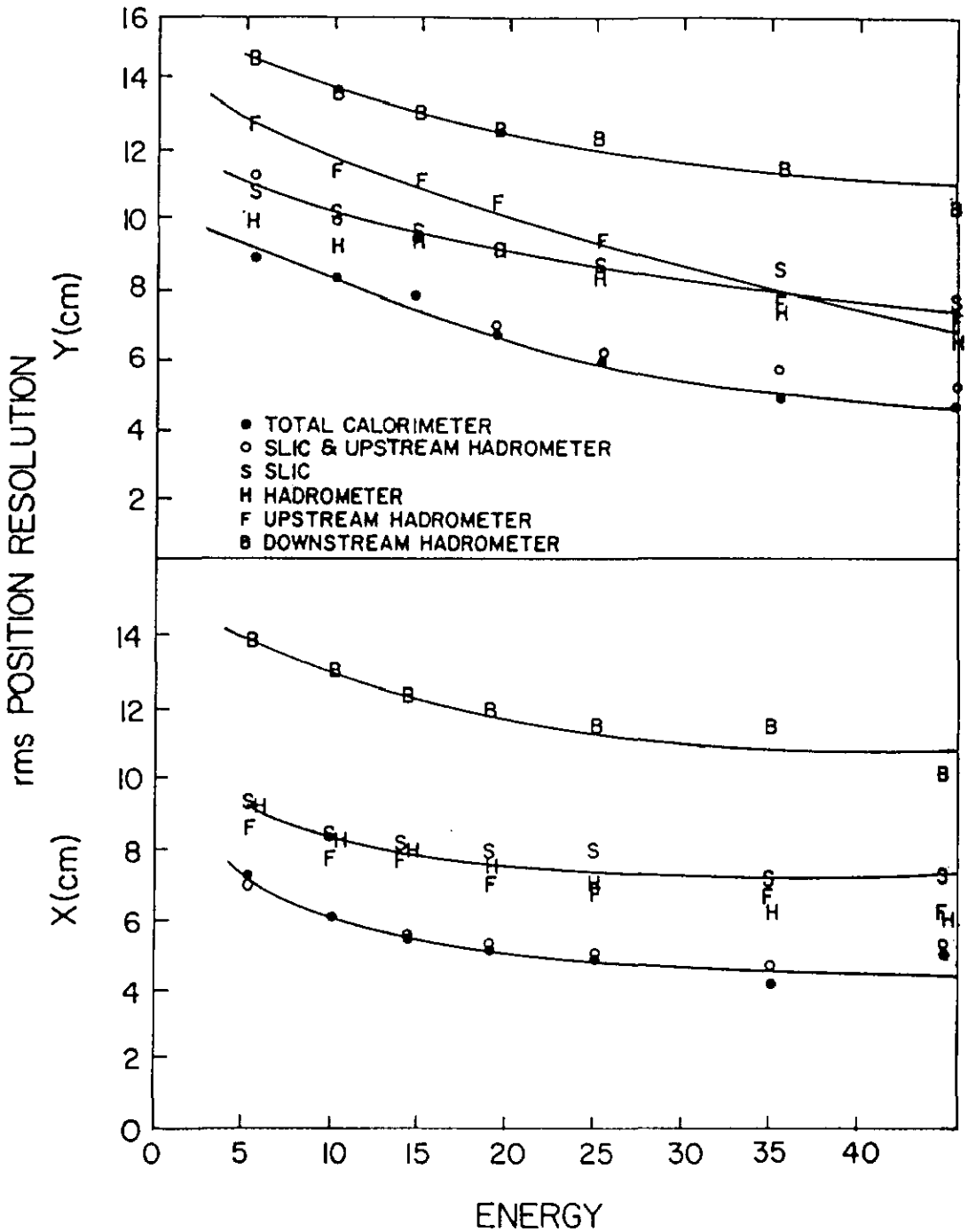

Figure 12

Position resolution (relative to incident trajectories) for isolated showers in horizontal (x) and vertical (y) directions versus energy (momentum).

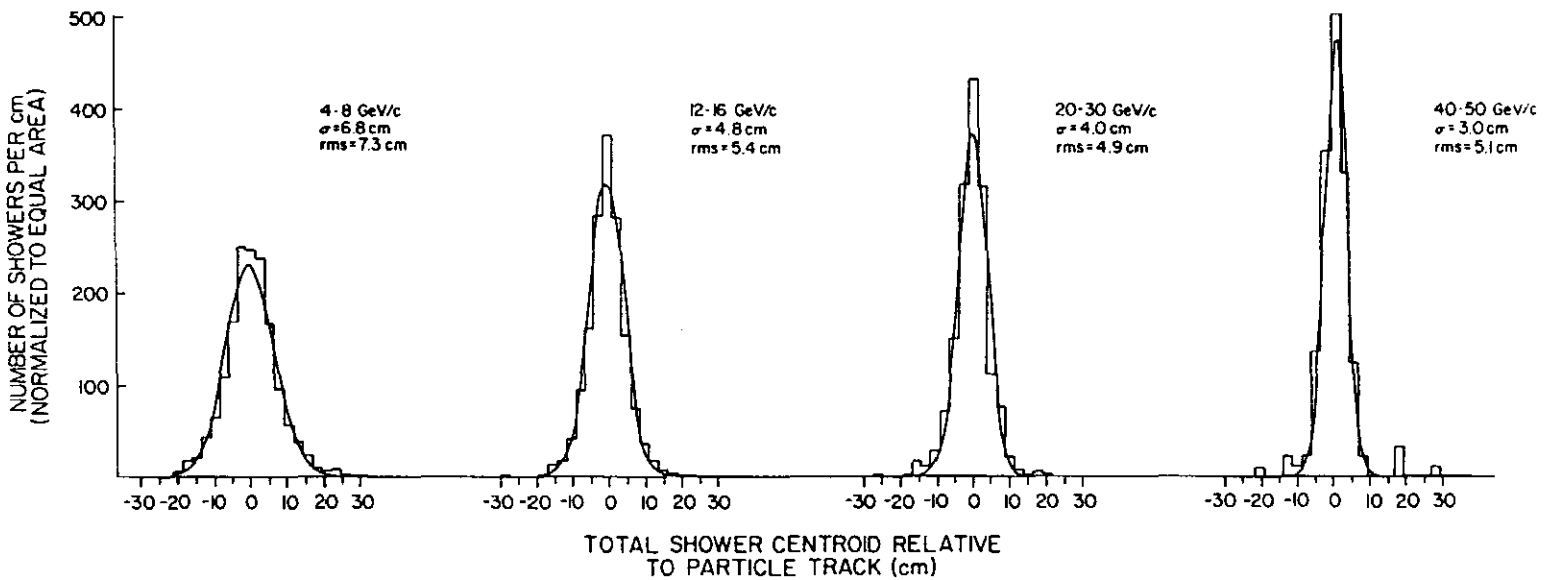

Figure 13

Typical position resolution curves in various momentum ranges from isolated showers in multiparticle events. The curves are fitted gaussians with the indicated σ width. The rms value is calculated directly from the data and used in Figure 12.

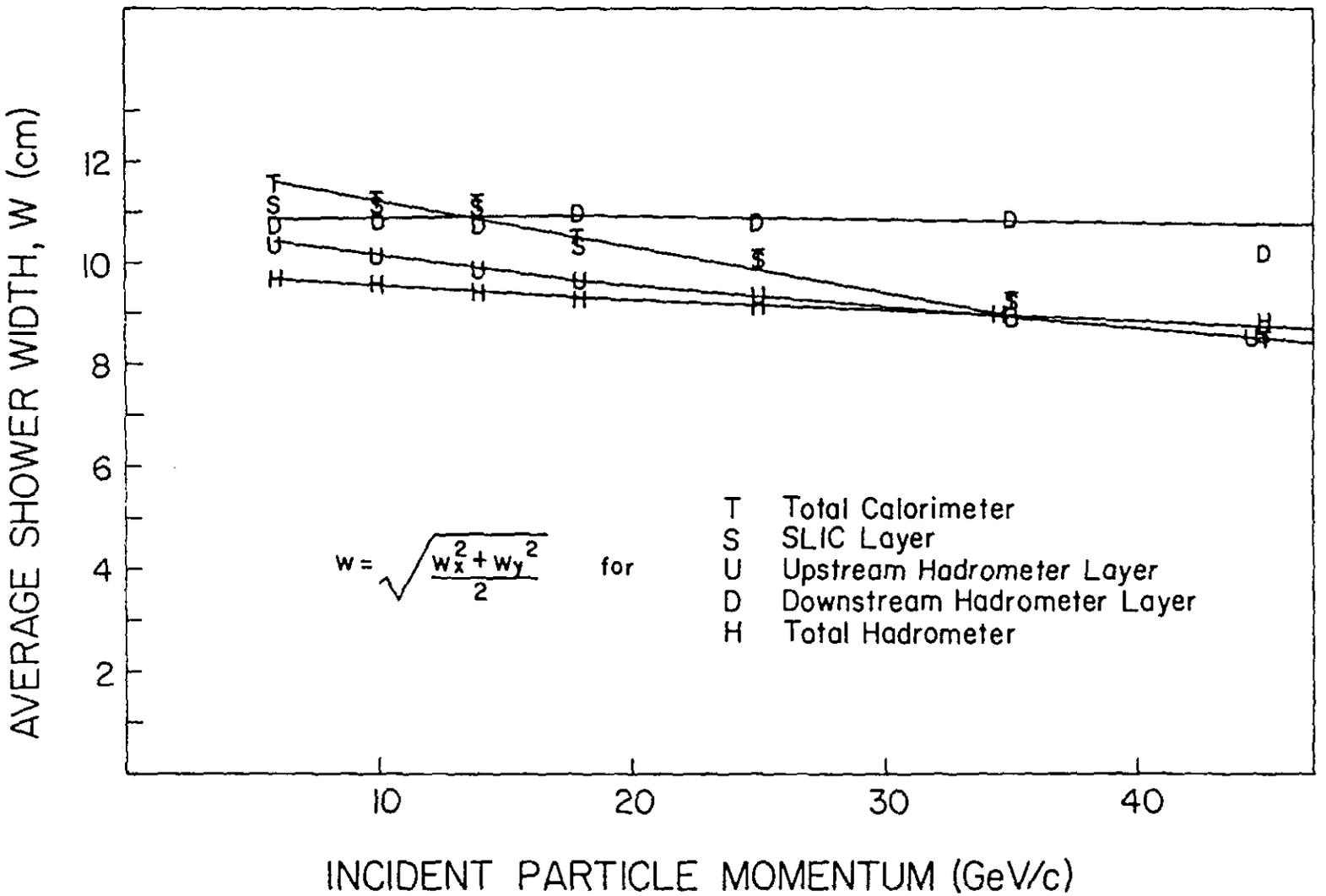

Figure 14

Hadronic shower width versus momentum from isolated showers due to charged particles with incident angles less than .03 radians in multiparticle events.

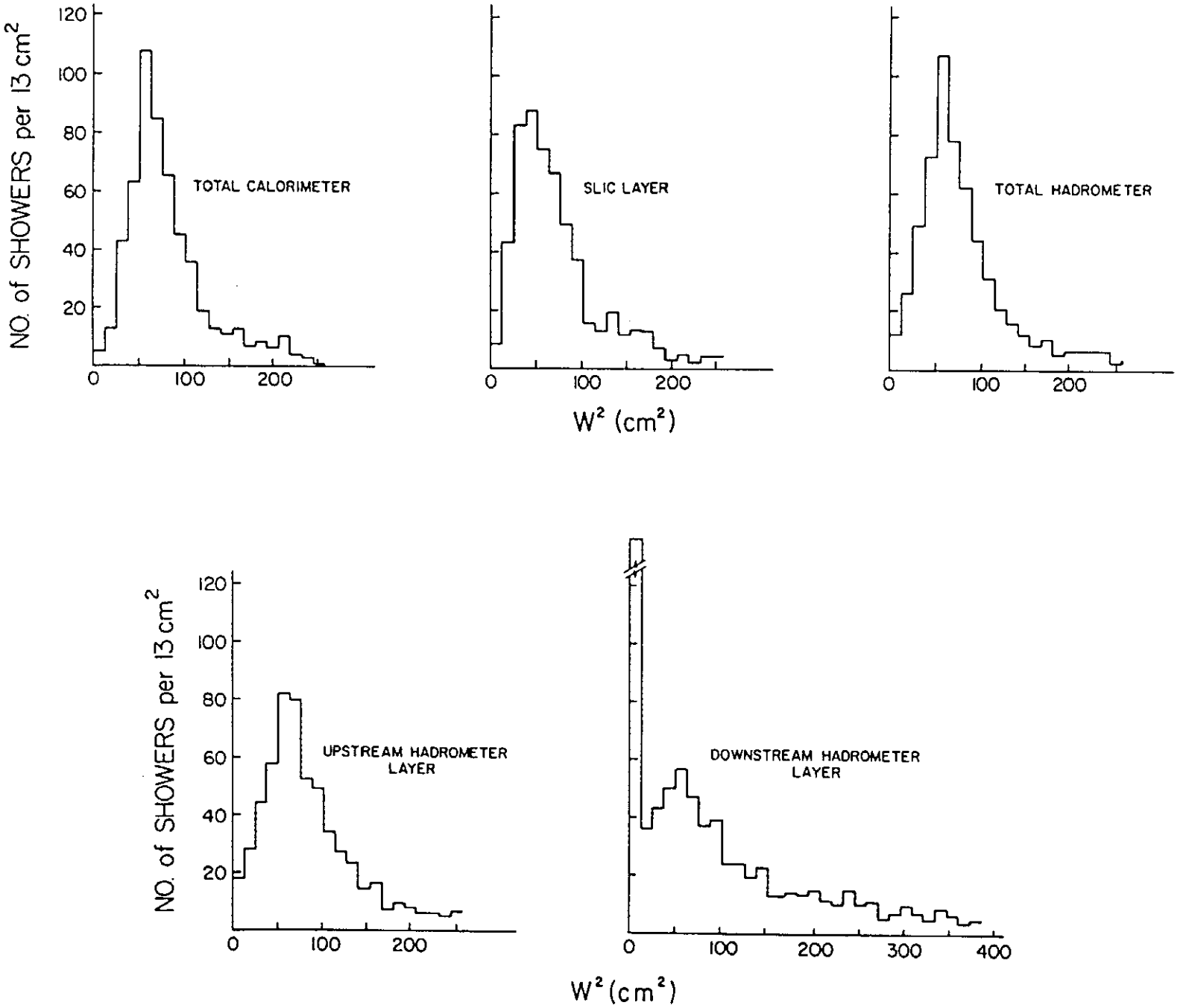

Figure 15

Hadronic shower width distributions for various calorimeter layers and combinations from isolated 20-30 GeV/c showers due to charged particles with incident angles less than .03 radians.

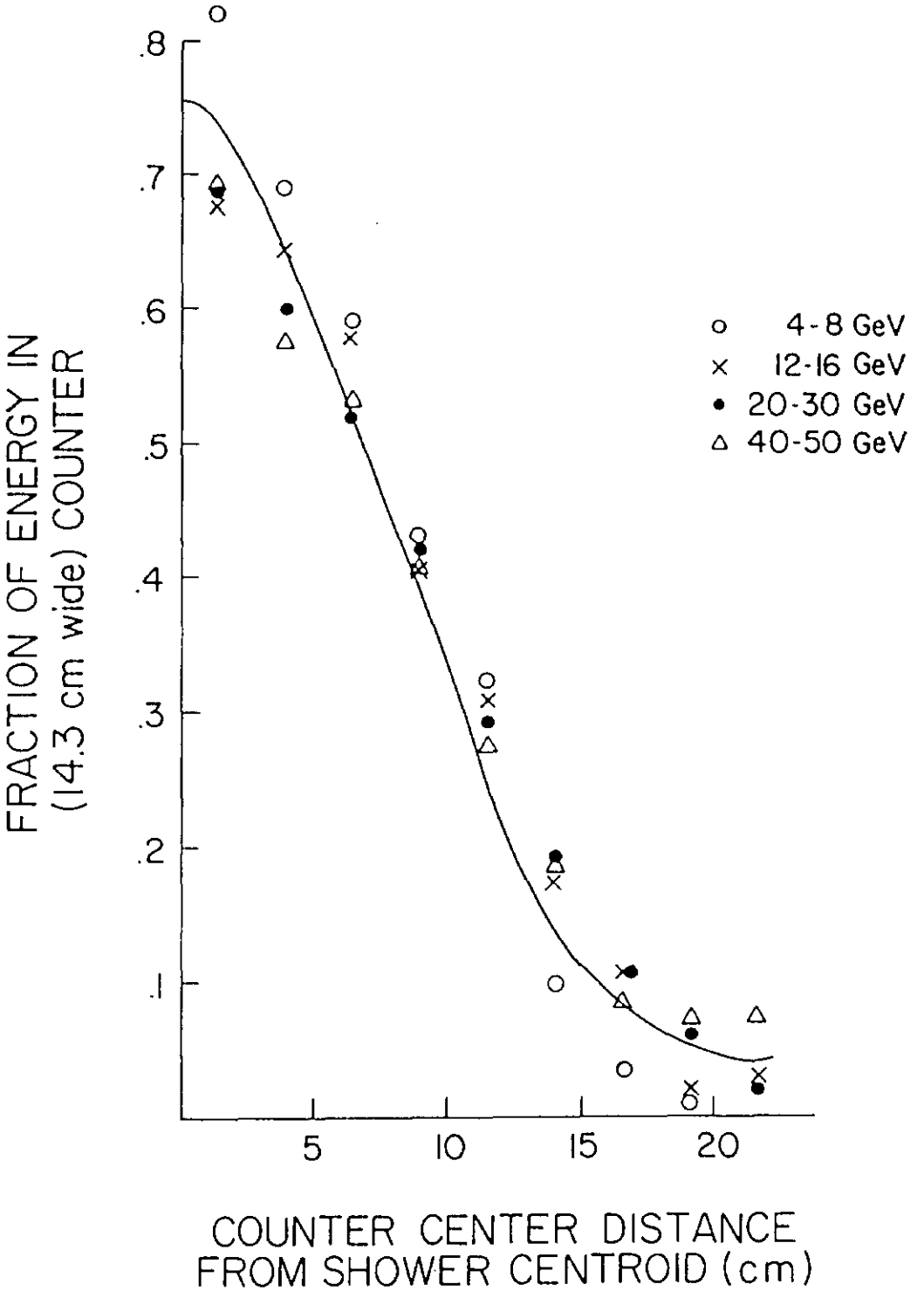

Figure 16

Neutral shower 'shapes' relative to shower centroid as seen by Hadrometer (front and back sum) at various incident energies. The curve is that for isolated charged hadrons relative to shower centroid.

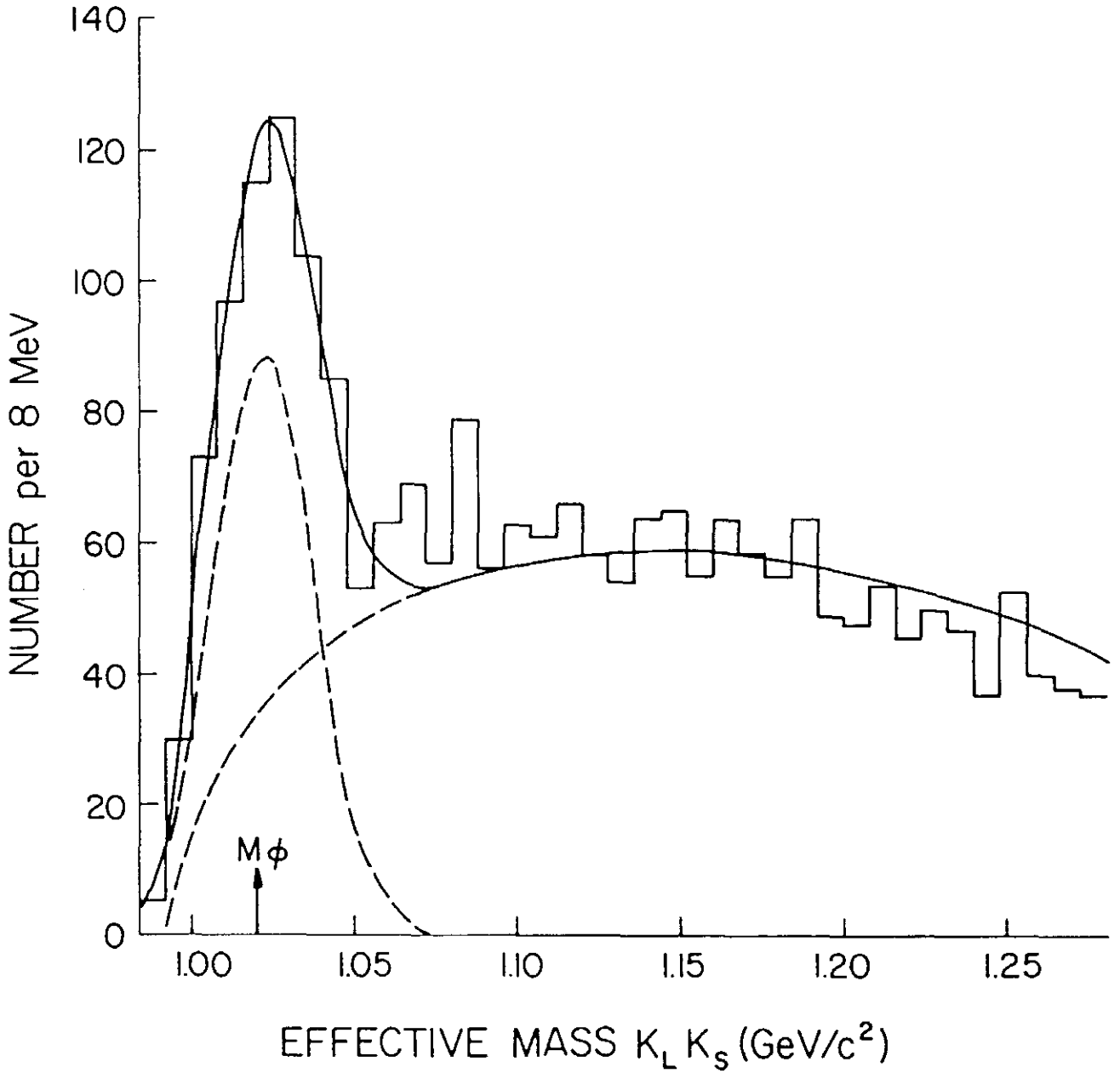

Figure 17

Effective mass distribution showing peak corresponding to $\phi \to K_S K_L$.

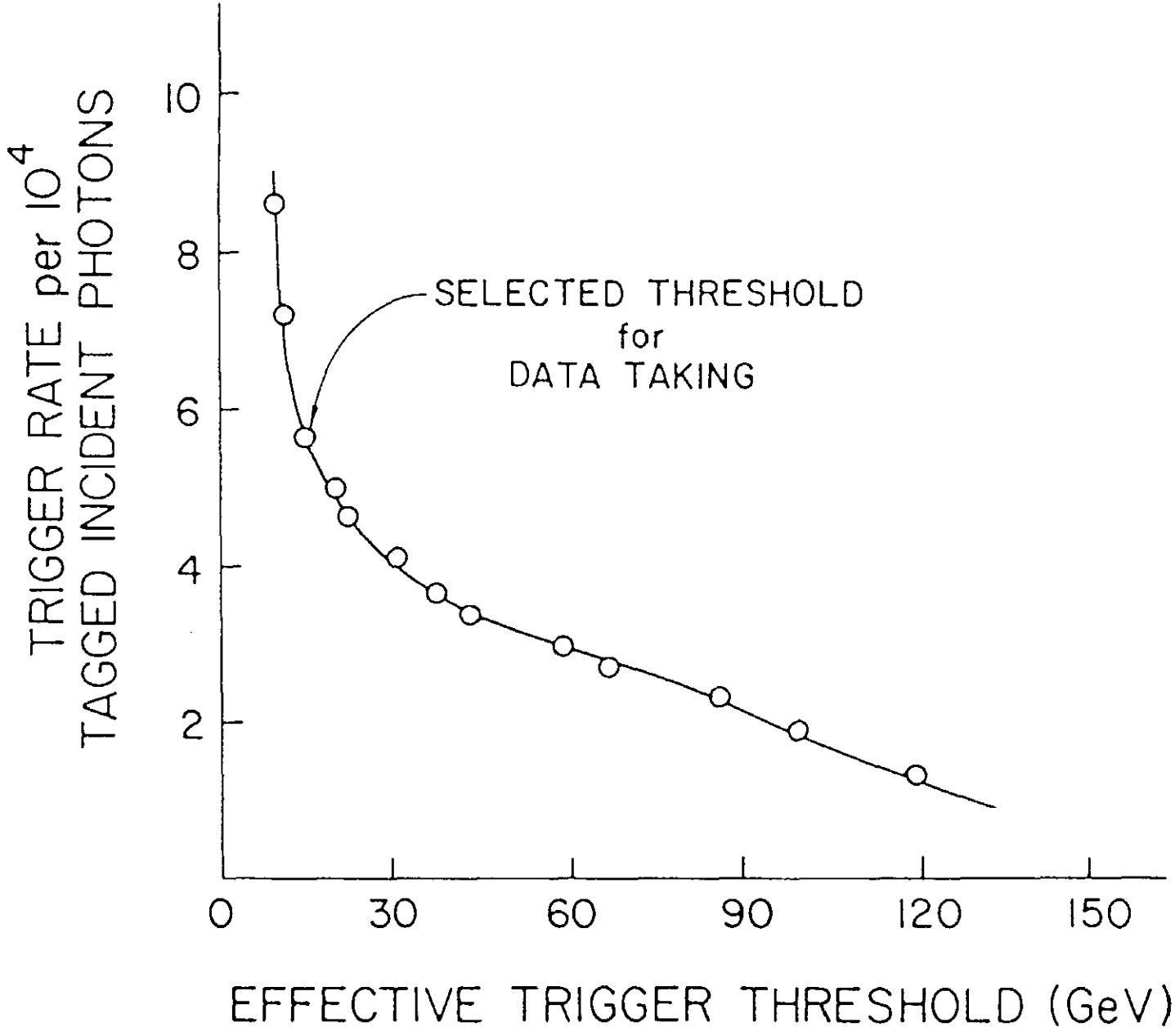

Figure 18

Trigger rate versus effective hadronic energy threshold in experiment running with incident tagged photons in the range 50-140 GeV.